J Appl Electrochem (2012) 42:517–526
DOI 10.1007/s10800-012-0429-x

ORIGINAL PAPER

Effects of lanthanum strontium cobalt ferrite (LSCF) cathode properties on hollow fibre micro-tubular SOFC performances

N. Droushiotis · A. Torabi · M. H. D. Othman · T. H. Etsell · G. H. Kelsall

Received: 28 March 2012 / Accepted: 1 May 2012 / Published online: 15 May 2012

Abstract Single layer $La_{0.6}Sr_{0.4}Co_{0.2}Fe_{0.8}O_3$ hollow fibre (HF) precursors (<1 mm ID) produced by phase inversion (PI) were sintered at 1,200, 1,350 and 1,400 °C. The increase in sintering temperature resulted in microstructural changes in the LSCF fibres, reflected in their electrical conductivities. LSCF-based cathodes with different designs were brushed onto co-extruded nickel–gadolinium-doped ceria (CGO) anode/CGO electrolyte dual-layer HFs (<1 mm ID) fabricated by PI. The effect of cathode layers on the overall performance of the fuel cells (FCs) was assessed using nearly identical anode and electrolyte compositions, thicknesses, and microstructures. Cathode microstructure design caused cells to perform differently producing peak power densities of 0.35–0.7 W cm^{-2} at 600 °C. Impedance spectroscopy analysis at 600 °C on the FCs produced 0.12–0.24 Ω cm^2 confirming the cathode's structural effect on the overall area-specific resistance of the FCs. The best performing FC with a brush-deposited cathode was compared to a similar FC where cathode was deposited by dip coating; at 600 °C the first produced 0.6 W cm^{-2} while the second cell 0.7 W cm^{-2}. Co-extruding anodes and electrolytes by using PI and combining dip coating for cathode deposition could lead to the fabrication of FCs with enhanced microstructures and improved performances.

Keywords Micro-tubular solid oxide fuel cells (SOFCs) · Phase inversion · Electrical conductivity · LSCF-based cathode · Brush-painted · Dip coating

1 Introduction

Solid oxide fuel cells (SOFCs) are efficient and environmentally benign converters of the chemical energy of fuels directly into electrical energy, using multilayer structures of a non-porous, gas impermeable, ionically conducting electrolyte sandwiched between a porous anode and cathode. The latter should be highly conducting, catalytically active for the reduction reaction, and thermally and chemically stable under oxidising conditions at high temperatures [1].

Mixed ionic–electronic conducting materials such as (La, Sr)CoO_3 have been identified as good candidate cathode materials for intermediate temperature (IT) SOFCs. Substituting iron for some of the cobalt to form $La_{1-x}Sr_xCo_{1-y}Fe_yO_{3-\delta}$ (LSCF) increases ion transport rates, electronic conductivities and oxygen reduction kinetics [2]. It is standard practice to develop composite cathodes consisting of LSCF and electrolyte material (e.g., cerium–gadolinium oxide, CGO), in an effort to produce suitably active cathodes for IT-SOFCs [3] and to decrease the difference in thermal expansion coefficients (TEC) between cathode and electrolyte layers (TEC of LSCF is ca. 15×10^{-6} K^{-1} [4] and TEC of CGO is ca. (12–13) × 10^{-6} K^{-1} [5]).

N. Droushiotis (✉) · M. H. D. Othman · G. H. Kelsall
Department of Chemical Engineering, Imperial College London, London SW7 2AZ, UK
e-mail: ndroushi@imperial.ac.uk

A. Torabi · T. H. Etsell
Department of Chemical and Materials Engineering, University of Alberta, Edmonton, AB T6G 2G6, Canada

M. H. D. Othman
Advanced Membrane Technology Research Centre (AMTEC), Universiti Teknologi Malaysia, 81310 Skudai, Johor, Malaysia

The cathode performance depends not only on the material, but also very much on its structure, which can be controlled during the fabrication process. In SOFCs, the methods of cathode fabrication depend largely on the cell configuration. For cathode-supported tubular cells, porous cathode tubes are first extruded and then sintered at high temperatures [6–8], as a procedure to develop an appropriate porosity and strength for the cathode substrate. For anode- and electrolyte-supported SOFCs, the cathode layer is usually deposited after preparing the anode/electrolyte assembly. This makes it possible to use various processes including slurry coating, screen printing, tape casting, and wet powder spraying for cathode deposition [9–12]. After deposition of the cathode slurry, it is dried and then sintered. In many cases, the sintering temperature can be lower for anode- and electrolyte-supported cells than for the cathode-supported type, giving higher surface area cathodes; therefore, these configurations are considered more favourable than the cathode-supported type. Physical processes such as vacuum plasma spraying have also been used to make cathodes by deposition onto a porous metallic felt substrate, and even for fabricating entire anode/electrolyte/cathode assemblies [13].

While the fabrication of cathode layers has been well studied for planar and tubular design SOFCs [14, 15], very few such reports have been found for micro-tubular configurations [16, 17]. Therefore, this work aimed to study the effect of cathode structure on cathode properties and micro-tubular SOFC performance. Three types of cathode layers were fabricated: (i) HFs of cathode material fabricated by conventional ram extrusion, (ii) paint-brushed and (iii) dip-coated, which were deposited onto well-developed electrolyte/anode dual-layer HFs. All three cathode types were then sintered at 1200, 1350 and 1400 °C, prior to being characterised by scanning electron microscopy and electrical conductivity and electrochemical measurements.

2 Experimental methods and materials

2.1 Fabrication of LSCF single layer hollow fibres

LSCF HFs were prepared by phase inversion (PI) followed by sintering, as described elsewhere [18]. The dope suspensions for spinning the HF membrane precursors were prepared firstly by dissolving a calculated quantity of polyethersulfone (PESf) with the additive polyvinylpyrrolidone (PVP) in the weighed amount of *n*-methyl-2-pyrrolidone (NMP) solvent in a ceramic container before the weighed amount of LSCF powder was then added gradually. The particulate dispersions were mixed in a ballmill for 48 h, degassed at room temperature under stirring and then loaded into two stainless steel syringes. They were extruded simultaneously by a syringe pump (PHD 2000 Programmable, Harvard Apparatus) through a spinneret into a tap water coagulation bath with de-ionised water as the internal coagulant. The HF precursors while forming were immersed in a water bath for more than 24 h to complete the solidification process.

To investigate the effect of sintering temperature on the microstructure and electrical conductivity of the cathode, the LSCF HFs were sintered (tube-type Carbolite VST-HST, UK) at 1200, 1350 and 1400 °C for 5 h.

2.2 Fabrication of NiO–CGO/CGO dual-layer HFs

Two ceramic suspensions for (a) anode inner layers and (b) electrolyte outer layers were prepared by slowly adding the dry oxide powders (i.e., CGO [$Ce_{0.9}Gd_{0.1}O_{1.95}$, surface area 35 $m^2\ g^{-1}$, d_{50} 0.32 μm] and nickel oxide [NiO, surface area 5 $m^2\ g^{-1}$, d_{50} 0.55 μm] (NexTech Materials Ltd., OH)) into a dimethylsulfoxide (DMSO) solution, in which a dispersant (polyethylene glycol 30-dipolyhydroxystearate) had already been dissolved. The required amount of polyethersulfone (PES) pellets was then added. The suspension components of the electrolyte/anode dual-layer HFs and the fabrication parameters are summarized in Table 1. The suspensions were degassed at room temperature, loaded into a stainless steel container and pressurized simultaneously through the triple orifice spinneret (1.2 mm/2.6 mm [inner layer]/3.5 mm [outer layer]) at an extrusion rate of 0.117 $cm^3\ s^{-1}$, into a tap water coagulation bath at 22 °C with a 0.20 m air-gap length. The internal coagulant was de-ionised water with a flow rate of 0.167 $cm^3\ s^{-1}$. The HFs were then sintered in air at 1,500 °C for 12 h in a tube furnace. More details about the fabrication technique are discussed elsewhere [19].

Table 1 Dual layer HF fabrication parameters

Component	Anode-supported micro-tubes	
	Inner layer	Outer layer
CGO	28.0 wt%	64.0 wt%
NiO	42.0 wt%	–
PESf	7.0 wt%	6.4 wt%
Additive	0.12 wt%	0.12 wt%
NMP	–	–
DMSO	22.88 %	29.48 %
Ethanol	–	–
PEG-400	–	–
Internal coagulant	De-ionised water	
External coagulant	Tap water	

2.3 Cathode deposition using paint brush

The deposition of the cathode slurry was done using a paint brush (Number 4, Toolzone flat artists' brushes) to paint the outer surface of the NiO–CGO/CGO dual-layer HF. Two different cathode pastes were made: a 50–50 wt% LSCF ($La_{0.6}Sr_{0.4}Co_{0.2}Fe_{0.8}O_3$, d_{50} 0.6 μm, Praxair Inc., USA)—CGO (10 mol% gadolinium-doped ceria, d_{50} 0.32 μm, NexTech Materials Ltd., USA) composite for the functional layer (FL), and pure LSCF for the current collector (CC). Ethylene glycol was used as the dispersant medium. After brushing the FL, it was dried in an oven (Elite Thermal Systems Ltd., UK) at 60 °C for 5 min. The current collector layer was then applied and dried similarly. Three cells were made with different cathode layers. Sample 1 was coated with just the FL and sample 2 with both the FL and current collector layer. These two samples were then sintered at 1,200 °C for 5 h. The third sample was fabricated differently using a two-step process. The first step involved coating three layers (2 FL and 1 CC) followed by sintering at 1,100 °C for 3 h. In the second step, another two layers of CC were deposited and then the sample was sintered at 1,200 °C for 5 h; this is summarized in Table 2.

2.4 Cathode deposition by dip coating

The LSCF–CGO cathode was coated on the outer surface of the NiO–CGO/CGO dual-layer HF by dip coating, as described in detail elsewhere [20]. The slurry was composed of inorganic powders (LSCF, Praxair, USA and CGO Fuel cell materials, Lewis Center, OH), dispersant (Menhaden fish oil, Tape Casting Warehouse, Yardley, PA), binder (polyvinyl butyral (PVB)), Tape Casting Warehouse, Yardley, PA) and solvents (azeotropic mixture of toluene and ethanol). Equal wt% of LSCF and CGO was mixed with 2.5 wt% of the dispersant and 10 wt% of the binder, and the solid loading was chosen to be 65 wt%. A two-step milling process was used in order to obtain homogeneous slurry and to minimize breakdown of the high molecular weight PVB molecules. Firstly, the inorganic powder, dispersant and solvent blend were mixed for 1 h using a planetary ball mill (Retsch, PM 100). The binder was then added and the milling continued for one more hour. Finally, the slurry was put under vacuum to remove the dissolved gas. The ceramic micro-tubes were thoroughly masked by PTFE tape except a 10 mm length in the centre which was to be coated by the slurry. The dip-coating rate was 0.33 m min^{-1}.

Table 2 Brush-painted cathodes onto NiO–CGO/CGO dual-layer HFs

Cathode coating/sample	Number/description of layers (after sintering) A: 50 %LSCF–50 %CGO B: pure LSCF
Cathode 1	1A
Cathode 2	2A/1B
Cathode 3	2A/1B + 2B (two-step coating)

2.5 Electrical conductivity measurements

The electrical conductivities of the LSCF cathodes were measured with the four-probe DC technique at 450–600 °C using a design described in detail elsewhere [21].

2.6 Single MT-HF-SOFC reactors

A silver wire (Alfa Aesar, UK) was twisted around the 25 mm long cathode and platinum paste (SPI Supplies Platinum Paint, USA) was used to attach the wire to the cathode. Silver wool was packed inside the HF to collect the current from the anode side. The wool was porous enough to minimise mass transfer limitations. The fabricated MT-HF-SOFC was attached to an alumina tube using high temperature cement (Aremco, USA) before being sealed in a quartz tube used as the air flow chamber. Details of the reactor and test apparatus used are given elsewhere [22]. The MT-HF-SOFC anode was supplied with controlled flows (ca. 15 cm^3 min^{-1}) of humidified hydrogen, while the cathode was supplied with a fixed air flow rate using mass flow controllers (Bronkhorst, UK). The nickel oxide was reduced to produce a Ni–CGO composite anode by flowing 5 cm^3 min^{-1} hydrogen through the lumen for 150 min at 550 °C. Electrochemical measurements were made using a Metrohm PGSTAT302 potentiostat/galvanostat with a 10 A current booster on MT-HF-SOFCs operating at temperatures between 500 and 600 °C in a tube furnace (Carbolite VST-HST 1200, UK).

3 Results and discussion

3.1 SEM analysis

(A) To investigate the effect of the cathode sintering profile on the cathode microstructure, LSCF HFs were sintered for 5 h at 1,200, 1,350 and 1,400 °C, with both heating and cooling rates of 5 °C min^{-1}. The samples were fractured and their microstructure imaged by SEM as shown in Fig. 1, which shows that, as expected, the porosity of the LSCF HFs was affected by sintering temperature. The high magnification images show that the particles sintered at 1,200 °C were small and the microstructure retained

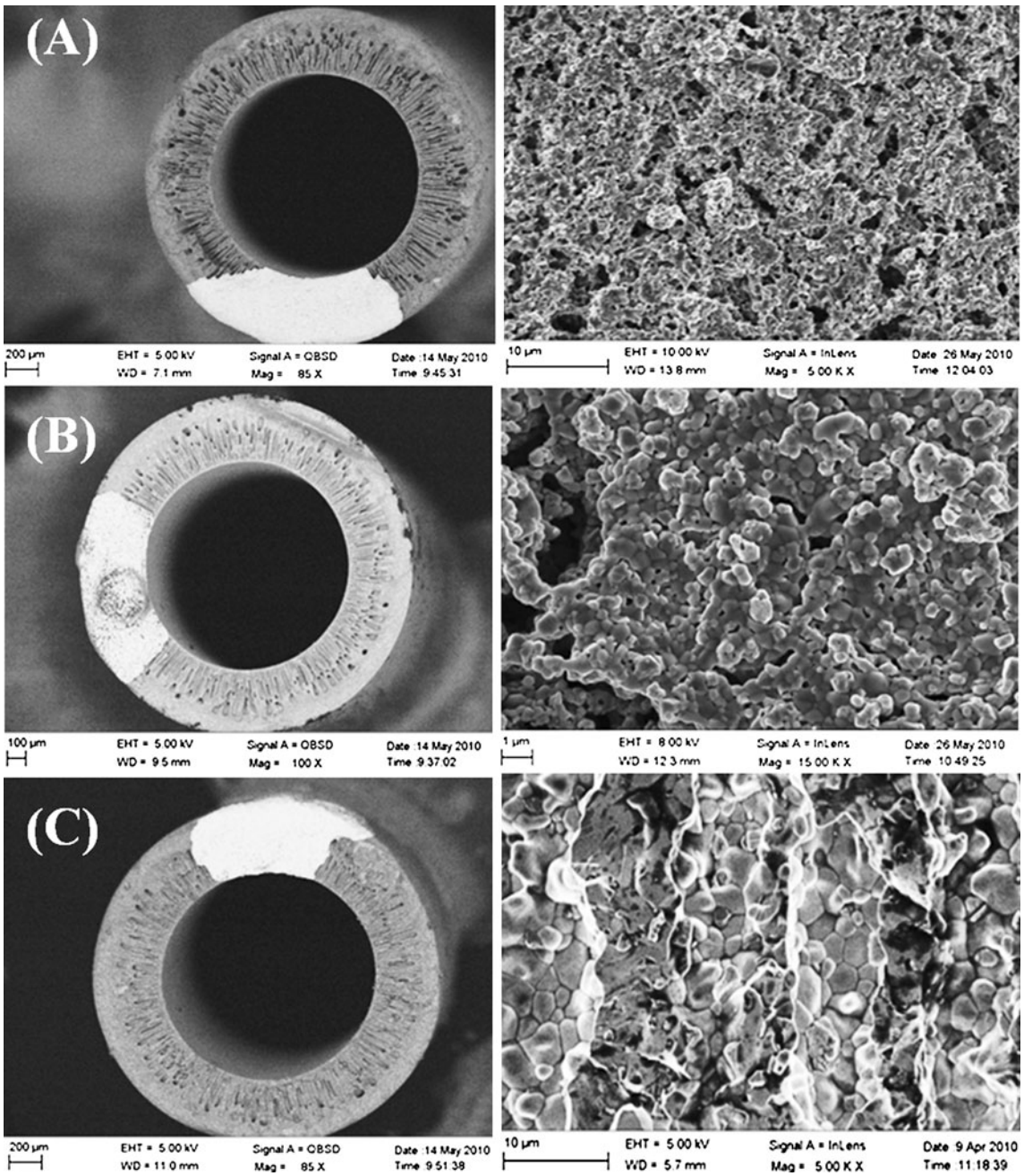

Fig. 1 SEM images of LSCF HFs sintered at different temperatures. **a** 1,200 °C, **b** 1,350 °C and **c** 1,400 °C

adequate porosity of ca. 20–30 %. However, as temperature was increased, ceramic particles became coarser and porosities decreased. At 1,400 °C, the membrane surface became smoother with distinct grain boundaries; grain sizes increased with temperature while most of the pores on the membrane surface disappeared. Furthermore, a similar study [23] on LSCF HFs found that increasing sintering temperatures can also increase phase impurities such as strontium sulphate within the LSCF, affecting its ionic and electronic conductivities. The effect of sintering temperature on the electrical properties of the LSCF HFs will be discussed in Sect. 3.2.

(B) To investigate the performance of different composite cathode electrodes (e.g., each cathode retained different thickness and microstructure) deposited onto similar (anode) Ni–CGO/CGO (electrolyte) dual-layer HFs previously sintered under identical conditions. Figure 2 shows SEM images of the complete fuel cells (FCs) with LSCF cathodes, as

specified in Table 2. Sample 1 had a <10 μm LSCF–CGO-coating (Fig. 2a), whereas sample 2 had a thicker FL of LSCF–CGO and a thin LSCF current collector layer (Fig. 2b); the darker and brighter particles in the FL are LSCF and CGO, respectively. However, it was not possible to use this technique with more than four deposition cycles to produce thicker cathodes with crack-free surfaces. In order to investigate the effect of thicker cathodes on Ni–CGO/CGO dual-layer HFs, a two-step process was utilised for sample 3 (Fig. 2c). Even though the final sintering temperature for the three samples was similar (i.e., 1,200 °C for 5 h), an intermediate sintering step at 1,100 °C for 3 h was used to fabricate sample 3. This two-step sintering affected the structure of the cathode layer and seemed to

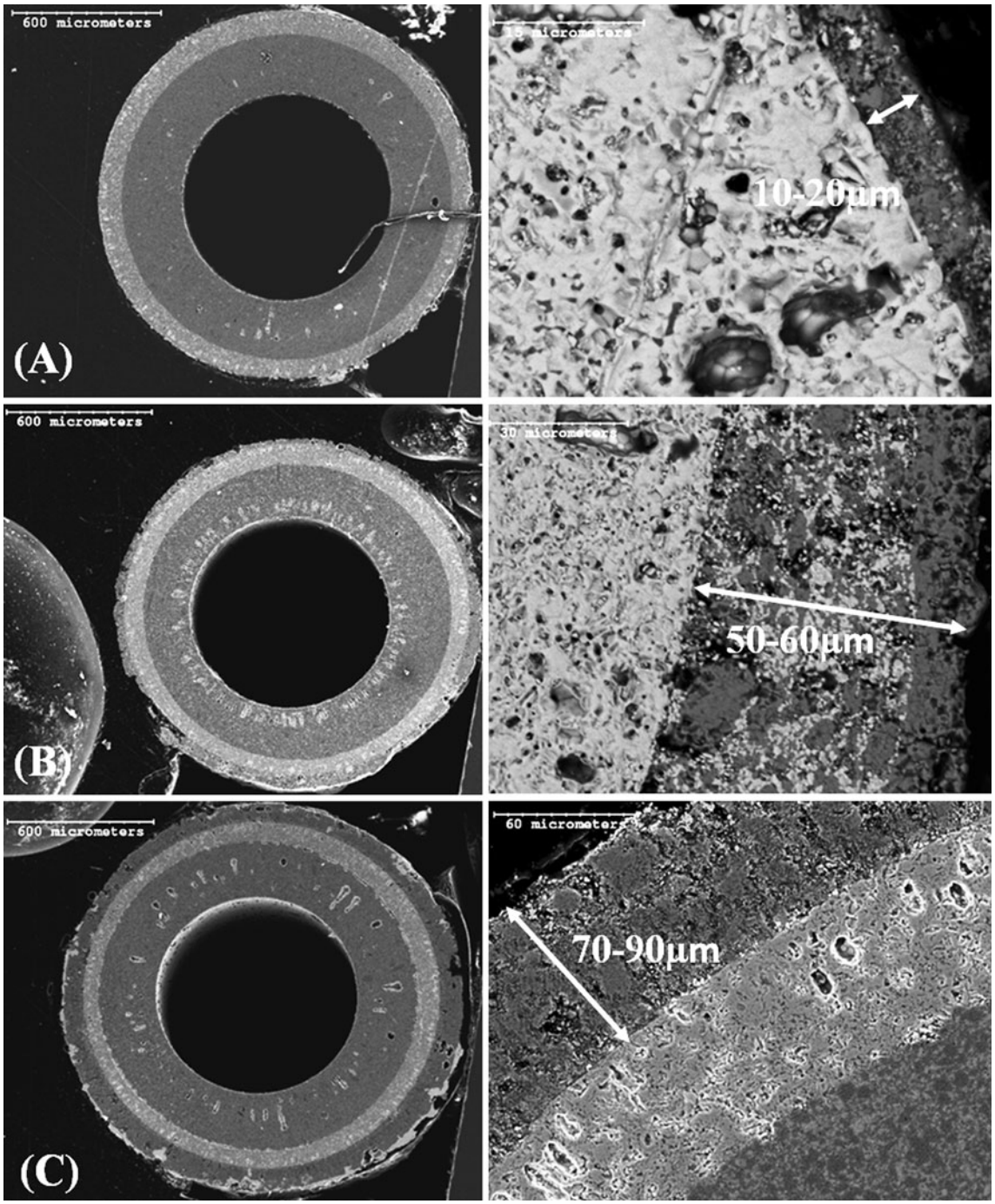

Fig. 2 SEM images of **a** cathode 1, **b** cathode 2 and **c** cathode 3

yield a denser coating, e.g., compared to sample 2 (Fig. 2b).

Furthermore, electrochemical kinetic measurements of samples 1–3, reported in Sect. 3.3 later, were made on the FCs for which cross sections are shown in Fig. 2. The brush-coated cathode of the best performing fuel cell (i.e., sample 2) was compared to a cathode of similar thickness, deposited by robotically controlled dip coating onto anode and electrolyte layers with similar microstructures and thicknesses; Figure 3 shows the SEM images of the two cross sections. The brush-coated cathode consisted of two distinct sub-layers (FL and current collector), while the dip-coated cathode layer consisted of only a FL. Figure 3 shows that the LSCF–CGO applied by dip coating was deposited consistently onto the Ni–CGO/CGO HFs and CGO–LSCF particles were distributed very uniformly along the cathode in contrast to the LSCF–CGO layer deposited by brush. In addition, the cathode layer deposited by dip coating was clearly much more adherent to the electrolyte layer with which it consequently formed a very smooth interface. In the case of the cathode applied by brush, the sharply demarcated interface between cathode and electrolyte could eventually cause their delamination.

3.2 Electrical conductivity

Figure 4 shows the temperature dependence of electrical conductivities of LSCF HFs sintered at different temperatures; conductivities increased with sintering temperature from 1,200 to 1,350 °C, but there was a significant decrease at 1,400 °C. In previous research on LSCF HFs [23], it was found that sintering temperatures above 1,350 °C not only caused changes to the crystalline structure, but also caused an increase of the average grain size of the LSCF. Based on the results presented in Fig. 4 microstructure changes [23] were probably responsible for the decrease in conductivity of the LSCF HFs at 1,400 °C. Hence, based on the electrical conductivities investigation it seems that sintering temperatures towards 1,200 and 1,350 °C favour the electrical properties of the cathode HFs. However, apart from the electronic properties, porosity and reaction area (three-phase boundary) are also key parameters for creating efficient electrodes. Further discussion on the performance of the cathodes will be analysed using impedance spectroscopy.

Figure 5 shows the temperature dependence of electrical conductivities of the different LSCF-based cathodes (cathode composition can be found in Table 2) deposited onto NiO–CGO/CGO dual-layer HFs. Compared to sample 1 (10 S cm^{-1}), sample 2 (35 S cm^{-1}) had improved electronic properties which seems may be due to the deposition of a current collector layer (pure LSCF coating) on top of the mixed CGO-LSCF layer. Furthermore, compared to sample 2, sample 3 (80 S cm^{-1}) retained higher electronic conductivity and this was probably due to the deposition of 2 extra pure LSCF coatings over the mixed CGO layers. It seems that this was due to the fact that, whereas a single layer coating deposited by paint brush retained a few microcracks, the deposition of a second layer resulted in a smoother surface. Microcracks can affect the LSCF continuity and hence the electrical conductivity of the cathode produced. Similar problems with coatings deposited by paint brush have been reported in previous research [24]. Based on the SEM images in Fig. 3 and the electrical conductivities in Fig. 5, cathode sample 2 was found to exhibit acceptable properties for application in MT-HF-SOFCs, not only due to its microstructure, but also due to the ease of fabrication and reproducibility of the deposition technique. However, the electrical conductivity of cathode sample 2, ca. 35 S cm^{-1}, was still an order of magnitude less than values reported in the literature [25, 26], possibly due to contact potential losses between the cathode and Pt current collector used for measuring the conductivity of the HFs at high temperatures and also probably due to differences between cathode structures and overall porosities (Table 3).

3.3 Fuel cell performance

Figure 6 shows the effects of current density on cell voltages and power densities for MT-HF-SOFCs with cathode samples 1, 2 and 3, which produced maximum power densities of ca. 0.38, 0.6 and 0.4 W cm^{-2}, respectively at 600 °C. Although cathode sample 3 had the highest electrical conductivity (Fig. 5), its power densities were lower than those for sample 2, due to the latter's greater porosity and possibly greater density of three-phase boundary lengths.

Figure 7 compares the effects of current density on cell voltages and power densities for MT-HF-SOFCs with the cathode deposited by dip coating and with brush-deposited cathode sample 2 operating at 600 °C. Interestingly, although the latter was composed of a FL and a current collector layer, the cathode with only a dip-coated FL performed better; 0.7 W cm^{-2} for dip-coated cathode (with 17 % fuel utilization on peak power density) and ca. 0.6 W cm^{-2} for brush-painted cathode (with 15 % fuel utilization on peak power density). Possible reasons include:

(a) The planetary ball milling used to produce the dip coating slurry of LSCF–CGO particles resulted in a very homogenous dispersion (Fig. 3) that achieved a substantially increased density of three-phase boundary lengths throughout the cathode.

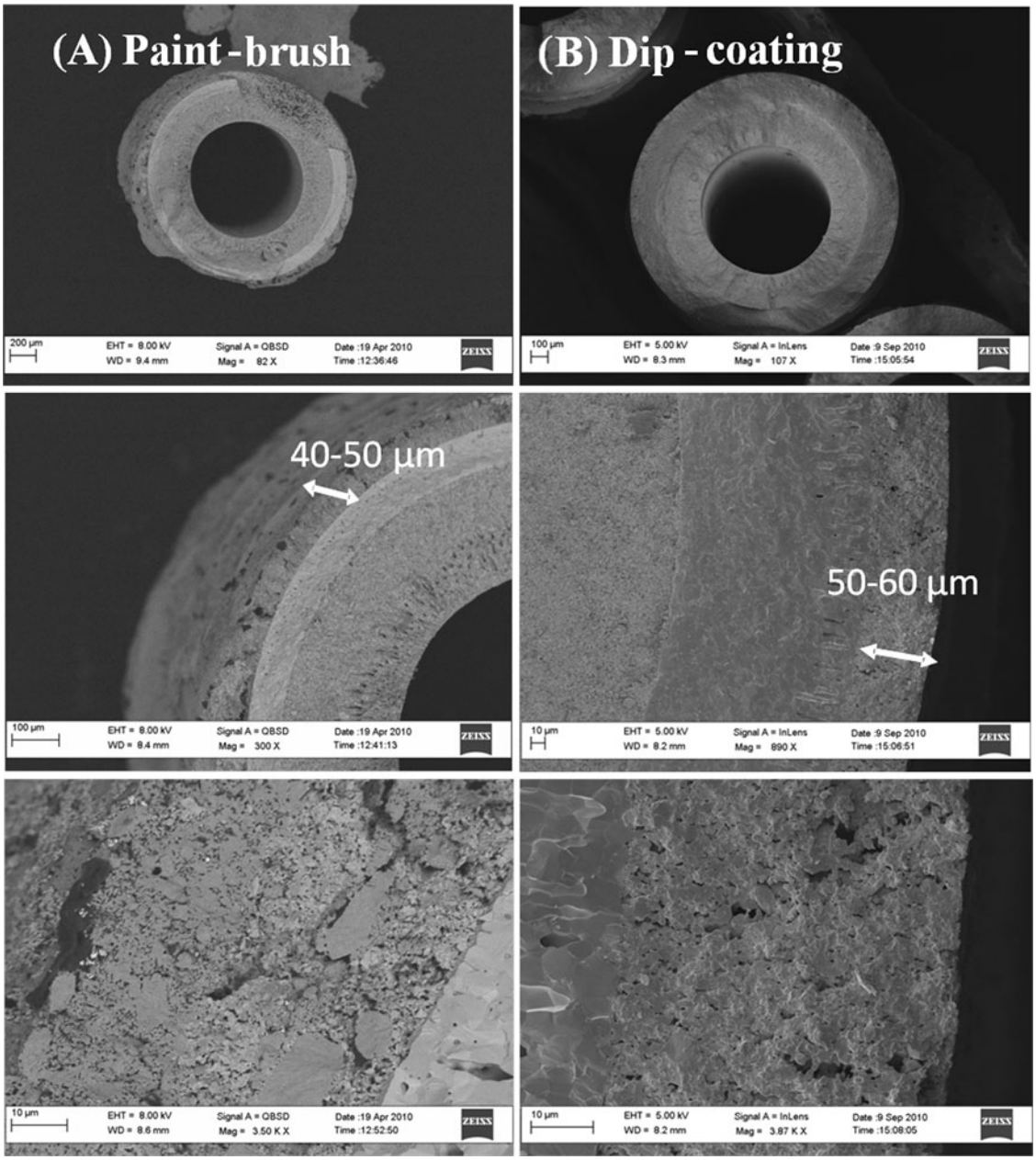

Fig. 3 **a** SEM images of cathode deposited using a paint brush and **b** by dip coating

(b) The adhesion between the cathode layer and the electrolyte was much stronger due to their very smooth interface in the dip-coated cathode.
(c) The thickness of the dip-coated cathode was highly uniform throughout the sample, unlike that of the brush-coated cathode.

Additionally, the dip-coating technique is much more controllable and reproducible; it could also be used to apply the LSCF current collector layer, possibly to improve the performance further.

3.4 Impedance spectroscopy

Figure 8 shows the impedance spectra for the MT-HF-SOFCs with cathode samples 1, 2 and 3 at 600 °C at open circuit. Though the spectra were obviously far from a combination of semi-circles, being strongly depressed due to the three-dimensional nature of the electrodes, the high frequency (10^4–10^5 Hz) intercept on the real axis enabled estimation of the temperature dependence of the Ohmic, ionic and electronic resistances in the electrolyte,

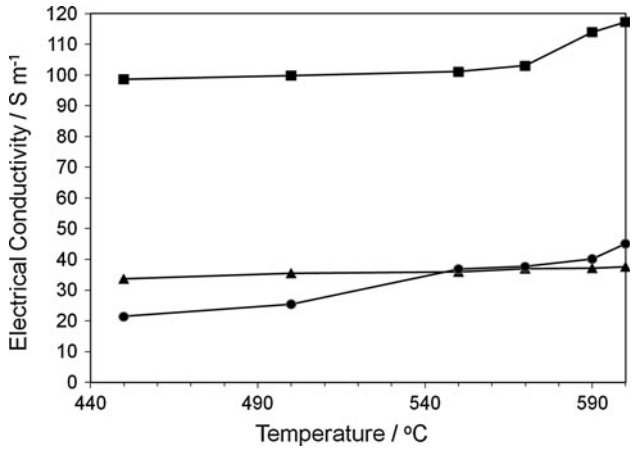

Fig. 4 Effect of sintering temperature on the electrical conductivity of LSCF fibres

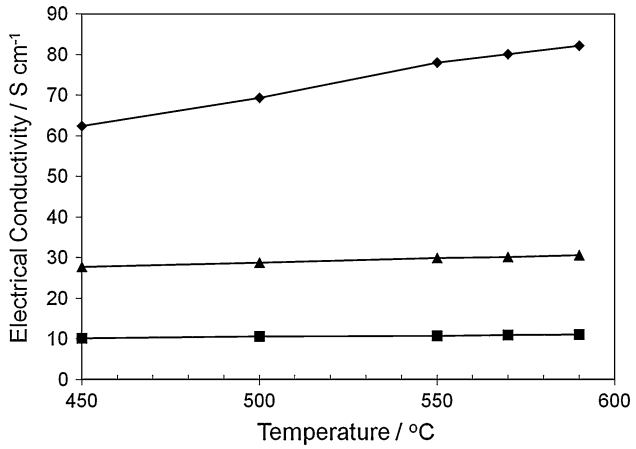

Fig. 5 Effect of temperature on electrical conductivities of the LSCF coatings

Table 3 Dimensions of the MT-HF-SOFCs and surface area of fuel electrode

Component	Number
Inner diameter (ID)	0.75 mm
Outer diameter (OD)	1.1 mm
Anode thickness	200–250 μm
Electrolyte thickness	70–90 μm
Cathode (brush-pained) thickness	40–50 μm
Cathode (dip-coated) thickness	50–60 μm
Active length (based on LSCF length)	1 cm
Active surface area (based on ID of fuel electrode)	ca. 0.236 cm^2

electrodes and current collectors. The low frequency (0.01–0.1 Hz) intercept on the real axis enabled estimation of the total impedance of the MT-HF-SOFCs including activation and concentration potential losses [19, 27, 28],

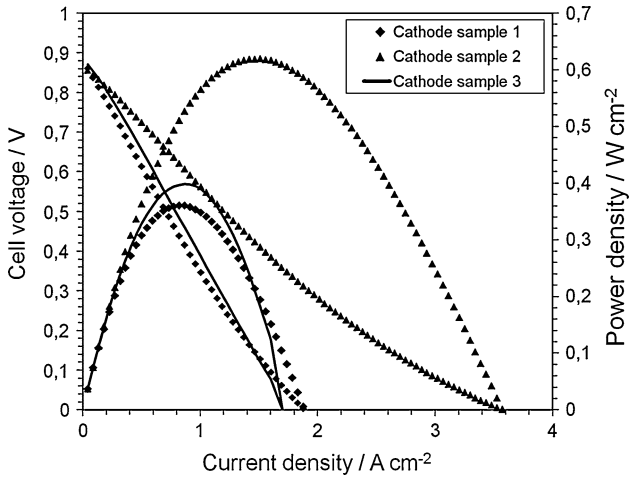

Fig. 6 Effect of current density on cell voltages and power densities of the dual-layer fibres with different cathode coatings at 600 °C

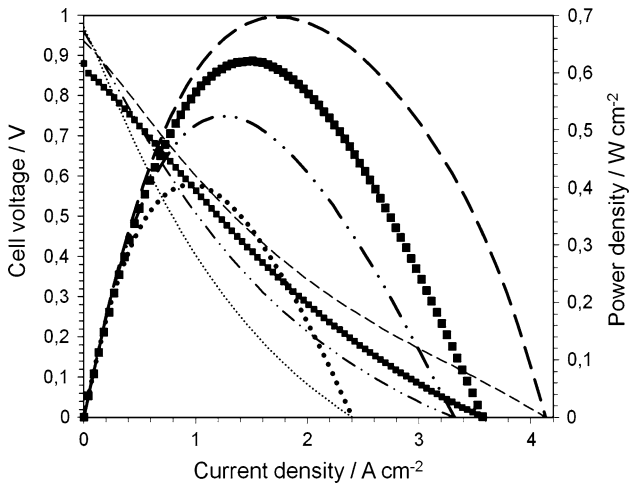

Fig. 7 Effect of current density on cell voltages and power densities of the HF-MT-SOFC consisting of a cathode deposited by dip coating

in addition to the Ohmic elements. Hence, the non-Ohmic losses caused by polarization within the cells can be derived, without differentiating between contributions from anode and cathode in the absence of three electrode measurements.

The objective of these measurements was primarily to investigate the effects of cathode fabrication conditions and microstructure on MT-HF-SOFC performance. As the anode and electrolyte were essentially the same for all three cells under open circuit conditions, differences among the impedance spectra in Fig. 8 reflected differences in the cathode layer. As expected from the performance data in Fig. 6 for the three cells, cell 2 exhibited the lowest Faradaic (and Ohmic) impedance, implying the thicker LSCF–CGO layer and higher porosity of its cathode coating resulted in a higher density of three-phase boundary lengths compared to cathode coatings 1 and 3. However, confirmation of this

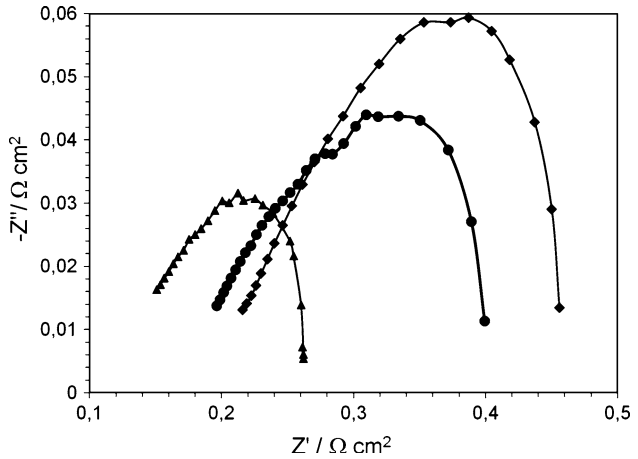

Fig. 8 Impedance spectra 0.01–10^5 Hz at 600 °C of the dual-layer fibres with different cathode coatings (samples 1–3) at open circuit

inference will require measurement of three-phase boundary lengths of different cathode coatings; those data would then be used within a finite element reactor model to predict the effects of cathode microstructure on the spatial distributions of current density and anode activation polarization, and global performance of MT-HF-SOFCs, as was reported previously [29] for the effects of anode microstructures.

4 Conclusions

(a) Recent literature has been reviewed on the fabrication techniques and materials for LSCF cathodes deposited onto ceria-based MT-HF-SOFCs and the effect of cathode coatings on fuel cell performance was reported.

(b) The sintering temperature of LSCF-based cathodes affect both their microstructures and electrical conductivities.

(c) LSCF-based cathodes with different designs and microstructures were deposited onto NiO–CGO/CGO dual-layer HFs by brush and sintered under similar conditions (i.e., at 1,200 °C). The thicknesses of the cathode FL and current collector layer and cathode microstructure affected the performance of complete MT–SOFCs, as determined from the effects of current density on cell voltages and power densities. Fuel cell peak power densities at 600 °C varied between 0.65–0.35 W cm^{-2} as cathode microstructure changed.

(d) Comparison of the performance of a MT-HF-SOFC with the optimum cathode paint-brushed with that of a MT-HF-IT-SOFC with a cathode deposited by dip coating showed the latter generated 15 % greater peak power density at 600 °C compared to the former. Dip coating of MT-HF-SOFC cathodes produced uniform deposits with strong adhesion to electrolyte layers that improved the catalytic activity of the cathode layer, resulting in better electrochemical performance compared with brush-painted cathodes.

Acknowledgments The authors thank the UK Engineering and Physical Sciences Research Council for a studentship for N.D. and the Natural Sciences and Engineering Research Council of Canada (NSERC), for funding the research. The authors also thank Dr B. Zydorczak for fabricating the LSCF HFs.

References

1. Minh NQ, Takahashi T (1995) Science and technology of ceramic fuel cells. Elsevier, Oxford
2. Brett DJL, Atkinson A, Brandon NP, Skinner SJ (2008) Intermediate temperature solid oxide fuel cells. Chem Soc Rev 37:1568
3. Esquirol A, Kilner J, Brandon NP (2004) Oxygen transport in $La_{0.6}Sr_{0.4}Co_{0.2}Fe_{0.8}O_{3-\delta}/Ce_{0.8}Ge_{0.2}O_{2-x}$ composite cathode for IT-SOFCs. Solid State Ionics 175:63
4. Lu L, Guo Y, Zhang H, Jin J (2010) Electrochemical performance of $La_2NiO_{4+\delta}$–$La_{0.6}Sr_{0.4}Co_{0.2}Fe_{0.8}O_{3-\delta}$ composite cathodes for intermediate temperature solid oxide fuel cells. Mater Res Bull 45:1135
5. Corbel G, Mestiri S, Lacorre P (2005) Physicochemical compatibility of CGO fluorite, LSM and LSCF perovskite electrode materials with $La_2Mo_2O_9$ fast oxide-ion conductor. Solid State Sci 7:1216
6. Takeuchi H, Nishiyama H, Ueno A, Aikawa S, Aizawa M, Tajiri H, Nakayama T, Suehiro S, Shukuri K (1999) In: Singhal SC, Dokiya M (eds) Solid oxide fuel cells VI, PV 99–19. The Electrochemical Society proceedings series, Pennington, p 879
7. Singhal SC (2000) Advances in solid oxide fuel cell technology. Solid State Ionics 135:305
8. Kuroishi M, Furuya S, Hiwatashi K, Tsujimoto K, Uchida Y, Yoshinaga H, Shukuri K (2001) In: Yokokawa H, Singhal SC (eds) Solid oxide fuel cells VII, PV 2001–16. The Electrochemical Society proceedings series, Pennington, p 88
9. Rietveld G, Nammensma P, Ouweltjes J P (2001) In: Yokokawa H, Singhal SC (eds) Solid oxide fuel cells VII, PV 2001–16. The Electrochemical Society proceedings series, Pennington, p 125
10. de Haart LGJ, Vinke IC, Janke A, Ringel H, Tietz F (2001) In: Yokokawa H, Singhal SC (eds) Solid oxide fuel cells VII, PV 2001–16. The Electrochemical Society proceedings series, Pennington, p 111
11. Yasuda I, Baba Y, Ogiwara T, Yakabe H (2001) In: Yokokawa H, Singhal SC (eds) Solid oxide fuel cells VII, PV 2001–16. The Electrochemical Society proceedings series, Pennington, p 131
12. Hattori M, Nakanishi A, Iio M (2001) In: Yokokawa H, Singhal SC (eds) Solid oxide fuel cells VII, PV 2001–16. The Electrochemical Society proceedings series, Pennington, p 1061
13. Schiller G, Franco T, Henne R, Lang M, Ruckdaschel R, Otschik P, Eicher IC (2001) In: Yokokawa H, Singhal SC (eds) Solid oxide fuel cells VII, PV 2001–16. The Electrochemical Society proceedings series, Pennington, p 895
14. Tietz F, Mai A, Stöver D (2008) From powder properties to fuel cell performance—a holistic approach for SOFC cathode development. Solid State Ionics 179:1509
15. Ivers-Tiffée E, Weber A, Schmid K, Krebs V (2004) Macroscale modeling of cathode formation in SOFC. Solid State Ionics 174:223

16. Liu Y, Hashimoto SI, Nishino H, Takei K, Mori M, Suzuki T, Funahashi Y (2007) Fabrication and characterization of micro-tubular cathode supported SOFC for intermediate temperature operation. J Power Sources 174:95
17. Zhang S, Bi L, Zhang L, Yang C, Wang H, Liu W (2009) Fabrication of cathode supported solid oxide fuel cell by multi-layer tape casting and co-firing method. Int J Hydrog Energy 34:7789
18. Tan X, Liu Y, Li K (2005) Preparation of $La_{0.6}Sr_{0.4}Co_{0.2}Fe_{0.8}O_{3-\delta}$ hollow fibre membranes for oxygen production by a phase-inversion/sintering technique. Ind Eng Chem Res 44:61
19. Droushiotis N, Doraswami U, Ivey D, Othman MHD, Li K, Kelsall GH (2010) Fabrication by co-extrusion and electrochemical characterization of micro-tubular hollow fibre solid oxide fuel cells. Electrochem Commun 12:792
20. Torabi A, Etsell TH, Sarkar P (2011) Dip coating fabrication process for micro-tubular SOFCs. Solid State Ionics 192:372
21. Droushiotis N, Doraswami U, Kanawka K, Kelsall GH, Li K (2009) Characterization of NiO-yttria stabilised zirconia YSZ hollow fibres for use as SOFC anodes. Solid State Ionics 180:1091
22. Droushiotis N, Doraswami U, Kelsall GH, Li K (2011) Micro-tubular solid oxide fuel cells fabricated from hollow fibres. J Appl Electrochem 41:1005
23. Tan X, Wang Z, Li K (2010) Effects of sintering on the properties of $La_{0.6}Sr_{0.4}Co_{0.2}Fe_{0.8}O_{3-\delta}$ perovskite hollow fiber membranes. Ind Eng Chem Res 49:2895
24. Du Y, Sammes NM (2004) Fabrication and properties of anode-supported tubular solid oxide fuel cells. J Power Sources 136:66
25. Jiang S (2008) Development of lanthanum strontium manganite perovskite cathode materials of solid oxide fuel cells: a review. J Mater Sci 43:6799
26. Tsipis E, Kharton V (2008) Electrode materials and reaction mechanisms in solid oxide fuel cells: a brief review. J Solid State Electrochem 12:1367
27. Orazem ME, Tribollet B (2008) Electrochemical impedance spectroscopy. Wiley, Canada
28. Othman MHD, Droushiotis N, Wu Z, Kanawka K, Kelsall G, Li K (2010) Electrolyte thickness control and its effect on electrolyte/anode dual-layer hollow fibres for micro-tubular solid oxide fuel cells. J Membr Sci 365:382
29. Doraswami U, Shearing P, Droushiotis N, Li K, Brandon NP, Kelsall GH (2011) Modelling the effects of measured anode triple-phase boundary densities on the performance of micro-tubular hollow fiber SOFCs. Solid State Ionics 192:494